doi:10.1016/j.jmb.2008.04.022 *J. Mol. Biol.* (2008) **379**, 1017–1028

JMB

Available online at www.sciencedirect.com

ScienceDirect

ELSEVIER

Structural Basis for Natural Lactonase and Promiscuous Phosphotriesterase Activities

Mikael Elias[1,2], Jérôme Dupuy[3], Luigia Merone[4], Luigi Mandrich[4], Elena Porzio[4], Sébastien Moniot[1], Daniel Rochu[5], Claude Lecomte[1], Mosè Rossi[4], Patrick Masson[5], Giuseppe Manco[4]* and Eric Chabriere[1,2,5]*

[1]*Laboratoire de Cristallographie et Modélisation des Matériaux Minéraux et Biologiques, CNRS-Université Henri Poincaré, 54506 Nancy, France*

[2]*Architecture et Fonction des Macromolécules Biologiques, CNRS-Université de la Méditerranée, 13288 Marseille, France*

[3]*Laboratoire de Cristallogenèse et Cristallographie des Protéines, Institut de Biologie Structurale JP EBEL, 38027 Grenoble, France*

[4]*Istituto di Biochimica delle Proteine, Consiglio Nazionale delle Ricerche, Via P. Castellino, 111, 80131 Napoli, Italy*

[5]*Unité d'Enzymologie, Département de Toxicologie, Centre de Recherches du Service de Santé des Armées, 38702 La Tronche, France*

Received 1 February 2008; received in revised form 3 April 2008; accepted 7 April 2008
Available online 16 April 2008

Edited by M. Guss

Organophosphates are the largest class of known insecticides, several of which are potent nerve agents. Consequently, organophosphate-degrading enzymes are of great scientific interest as bioscavengers and biodecontaminants. Recently, a hyperthermophilic phosphotriesterase (known as *Sso*Pox), from the Archaeon *Sulfolobus solfataricus*, has been isolated and found to possess a very high lactonase activity. Here, we report the three-dimensional structures of *Sso*Pox in the apo form (2.6 Å resolution) and in complex with a quorum-sensing lactone mimic at 2.0 Å resolution. The structure also reveals an unexpected active site topology, and a unique hydrophobic channel that perfectly accommodates the lactone substrate. Structural and mutagenesis evidence allows us to propose a mechanism for lactone hydrolysis and to refine the catalytic mechanism established for phosphotriesterases. In addition, *Sso*Pox structures permit the correlation of experimental lactonase and phosphotriesterase activities and this strongly suggests lactonase activity as the cognate function of *Sso*Pox. This example demonstrates that promiscuous activities probably constitute a large and efficient reservoir for the creation of novel catalytic activities.

Keywords: lactonase; phosphotriesterase; hyperthermophilic enzymes; 3D structure; active-site mutants

**Corresponding authors.* G. Manco is to be contacted at Istituto di Biochimica delle Proteine, Consiglio Nazionale delle Ricerche, Via P. Castellino, 111, 80131 Napoli, Italy. E. Chabriere, Architecture et Fonction des Macromolecules Biologiques, CNRS-Universite de la Mediterranee, 13288 Marseille, France. E-mail addresses: g.manco@ibp.cnr.it; eric.chabriere@afmb.univ-mrs.fr.

Abbreviations used: PEG, polyethylene glycol; PTE, phosphotriesterase; *Sso*Pox, *Sulfolobus solfataricus* phosphotriesterase; PLL, phosphotriesterase-like-lactonase; Opd, organophosphorus degrading; OP, organophosphates; rmsd, root-mean-square deviation; AHL, *N*-acyl-homoserine lactone; AhlA, *N*-acyl homoserine lactone acylase from *Rhodococcus erythropolis*; OpdA, phosphotriesterase from *Agrobacterium radiobacter*; C10 HTL, *N*-decanoyl-L-homocysteine thiolactone; C8 HSL, N-octanoyl-L-homoserine lactone.

Introduction

Organophosphates (OPs) are well-known potent toxic compounds that inhibit acetylcholinesterase irreversibly, a key enzyme of the central nervous system. They have been used extensively since the end of World War II. Their toxic properties have been exploited for the development of chemical warfare agents such as sarin, soman and VX, and principally for the development of agricultural insecticides.[1] Enzymes that are capable of degrading these OPs are therefore attractive as potential antidotes for both organophosphate-based pesticides and nerve agents.[2] Enzymatic detoxification of OPs has become the subject of numerous studies because current methods of removing them, such as treatment with bleach and incineration, are slow, expensive and cause environmental concerns. For this application, OP hydrolases are appealing due to their broader substrate specificity and higher catalytic rate.[2]

Phosphotriesterases (PTEs) are members of the amidohydrolase superfamily,[3] enzymes catalyzing hydrolysis of a broad range of compounds with different chemical properties (phosphoesters, esters, amides, etc.). Their coding genes, *opd*s (*o*rgano *p*hosphate *d*egradation), were isolated from *Pseudomonas diminuta*,[4] *Flavobacterium* sp.,[5] *Agrobacterium radiobacter*,[6] and genes similar to *opd* were also located in Archaea.[7] Since synthesis of their most efficient substrate, known as paraoxon, was described in the 1950s, it has been postulated that phosphotriesterases might have evolved specifically to this high level of catalytic efficiency over a relatively short period of time.[8] Several PTE structures are available in the PDB database, including those from *P. diminuta*,[9] and a very similar (90% sequence identity) OpdA homologue from *A. radiobacter*.[10] PTEs are $(\beta/\alpha)_8$-barrels and have a binuclear metal centre located at the C-terminal end of the barrel.[9,10] These enzymes show a high catalytic turnover, and their activity is modulated by the presence of divalent metal cations. It has been reported that the most active isoenzyme is Co^{2+}-substituted PTE.[11] Although complete active site metal substitution has been described,[9] recent results using anomalous fluorescence have shown both an incomplete metal substitution and a potential role for an iron cation (Fe^{2+}) in catalysis.[12] A catalytic mechanism for the hydrolysis of phosphotriesters has been proposed,[13] and it is reviewed in the present article.

A protein from the hypertermophilic archaeon *Sulfolobus solfataricus*, *Sso*Pox, has recently been cloned and characterized for its phosphotriesterase activity.[7] Although it displays only about 30% sequence identity with mesophilic PTEs, all amino acids coordinating the binuclear metal-centre are conserved. Furthermore, *Sso*Pox catalyzes the hydrolysis of paraoxon and other pesticides with a lower efficiency. Similar to the *Pseudomonas* PTE, its activity depends on the presence of metal ions, with cobalt significantly enhancing catalysis.[7] *Sso*Pox has been proved to have a high level of thermal stability, with denaturation half-lives (T_m) of 4 h and 90 min at 95 °C and 100 °C, respectively. This property allows rapid high-yield purification of the recombinant enzyme by simply heating cell lysates and thus precipitating host proteins. Owing to its exceptional stability, this PTE may be an excellent candidate in biotechnological studies seeking an efficient biodecontaminant of organophosphorus compounds.

Recently, a high level of catalytic activity and specificity with lactones as substrates has been reported for *Sso*Pox. Afriat and co-workers [14] proposed *Sso*Pox, *N*-acyl-homoserine lactone acylase from *Rhodococcus erythropolis* (AhlA) and the putative parathion hydrolase from *Mycobacterium tuberculosis*, to be members of a new group of enzymes dubbed phosphotriesterases-like-lactonases (PLLs), based on the observation of sequence features not present in mesophilic PTEs and the recognition of significant differences in enzyme specificity. In particular, the activity detected against natural homoserine lactones may relate these proteins to a precise biological function. Indeed, cell-to-cell communication mediated by small diffusible molecules is a common occurrence in several bacteria,[15] a phenomenon known as quorum sensing. For example, many Gram-negative bacteria use *N*-acyl-homoserine lactones (AHLs) as signalling molecules that regulate gene expression patterns, which in turn allow the bacteria to display "group behaviour". Displaying a high level of activity against AHLs, PLLs could have a role in these signalling pathways as well,[14] or be involved simply in the utilization of these compounds as a carbon and energy supply.

Here, we report the crystallographic structures of the hyperthermophilic *Sso*Pox in its apo form at 2.6 Å and in complex with a quorum-sensing lactone mimic at 2.0 Å. The structure identifies this enzyme as the prototype of the newly identified PLL family. The structural analysis permits us to propose a lactonase mechanism, to refine the previously proposed catalytic mechanism for PTEs and, by adding data supporting the hypothesis that the *Sso*Pox lactonase activity is in fact its native function, to exemplify the promiscuous relationship between lactonases as *Sso*Pox and optimized phosphotriesterases.

Results

X-ray structure of the hyperthermophilic phosphotriesterase

The structure of *Sso*Pox was refined at 2.6 Å resolution (Table 1). *Sso*Pox is homodimeric, and the monomer is roughly globular with overall dimensions of approximately 40 Å × 54 Å × 46 Å. *Sso*Pox displays only about 30% identity with the two other known mesophilic PTEs,[7] but its topology is similar. The *Sso*Pox structure could be described as a distorted $(\beta/\alpha)_8$ barrel. The structures superimpose well with a root-mean-square deviation (rmsd) for α-carbon atoms between *Sso*Pox and *P. diminuta* PTE (over 268 atoms) and *Sso*Pox and *A. radiobacter* PTE (over 271 atoms) of 1.05 Å and 1.11 Å, respectively.

Table 1. Data collection and refinement statistics

	Native	Complex
A. *Data collections*		
Wavelength (Å)	0.979	0.934
Resolution (Å)	2.6	2.05
Space group	$P2_12_12_1$	$P_1\ 2_12_1$
Unit cell dimensions		
a (Å)	87.16	86.38
b (Å)	104.82	104.12
c (Å)	155.36	153.05
No. observed reflections	334,245 (34293)	610,050 (75603)
No. unique reflections	43,406 (4438)	84,107 (10644)
Completeness (%)	97.6 (94.5)	96.5 (92.8)
R_{merge} [a] (%)	9.8 (33.6)	13.6 (40.5)
$R_{measured}$ [b] (%)	11.1 (52.2)	13.8 (66.8)
$I/\sigma(I)$	17.59 (4.49)	13.66 (3.98)
Last resolution shell	2.60–2.70	2.05–2.15
Redundancy	7.70 (7.72)	7.25 (7.10)
B. *Refinement statistics*		
Resolution range (Å)	46.42–2.60	86.07–2.05
No. reflections	44,340	82,757
R_{free} / R_{work} [c]	29.9/24.0 (34.0/31.0)	28.2/22.8 (37.0–30.0)
No. protein atoms	10,108	10,108
No. water molecules	239	762
Average *B* factor (Å^2)	38	28.7
rmsd from ideal		
Bond lengths (Å)	0.006	0.007
Bond angles (°)	1.061	1.153

Values in parentheses are for the last bin.

[a] $R_{sym} = R_{merge} = \sum_h \left| \hat{I}_h - I_{h,i} \right| / \sum_h \sum_i^{nh} I_{h,i}$.

[b] $R_{meas} = \sum_h \sqrt{\frac{n_h}{n_h - 1}} \sum_i^{n_h} \left| \hat{I}_h - I_{h,i} \right| / \sum_h \sum_i^{n_h} I_{h,i}$ · with $\hat{I}_h = \frac{1}{n_h} \sum_i^{n_h} I_{h,i}$.

[c] $R_{work} = \sum \| F_o - |F_c| \| / = \sum |F_o|$ where F_o denotes the observed structure factor amplitude and F_c, the structure factor amplitude calculated from the model. R_{free} is as for R_{work} but calculated with 5% of randomly chosen reflections omitted from the refinement.

Some major structural differences are illustrated in Fig. 1a. There are two shortenings of the *Sso*Pox polypeptide chain compared to the mesophilic PTE structures. The first is located in the vicinity of the active site entry and consists of the loss of a 15 residue loop, which corresponds to loop 7 in the $(\beta/\alpha)_8$ barrel topology. The other is the shortening of both extremities of the polypeptide chain. In fact, there are six and two residues less at the C terminus extremity, and two and four residues less at the N-terminal extremity, compared to *P. diminuta* PTE and *A. radiobacter* PTE, respectively. In addition, loop 8 of *Sso*Pox is more detached from the protein core, compared to the mesophilic proteins. Finally, an additional modification consists of the presence of extra loops involved in dimerization of the enzyme.

Description of the active site

Description of the free-enzyme

Similar to the mesophilic PTEs, the *Sso*Pox active site consists of a cavity containing a binuclear centre (Fig. 1b), located at the C terminus of the β-barrel.[10,16] These two metal cations are bridged by a putative catalytic water molecule, and by a carboxylated lysine. As for the metal cation coordination, four histidine residues are also involved, as well as an aspartic acid (Asp256) and a second water molecule. The most deeply buried metal cation (called α) adopts a trigonal bipyramidal geometry, being bound by coordination bonds with His22, His24, Asp256, Lys137 and the bridging water molecule. The most solvent-exposed (called β) has a distorted trigonal bipyramidal geometry, and is bound to His170, His199, Lys137, the bridging water molecule and the second water molecule. The bridging water molecule is almost equidistant from both metal cations, with a short distance contact (about 2 Å), and is hydrogen bonded with Asp256 (2.68 Å). In *Sso*Pox, the binuclear centre, the four histidine residues, the aspartic acid, and the carboxylated lysine are conserved and well superimposed with the mesophilic PTE structures (Fig. 1a). Those two metal cations are bound as in the mesophilic PTEs.[9] Structural comparison with the two other PTEs led to the identification of amino acids similar to those involved in the phosphotriester binding of bacterial PTEs.[15] The phosphotriester binding site was verified by docking with a phosphotriester mimic, namely diethyl-4-methylbenzylphosphonate (Fig. 2). Thorough structural comparison shows that the chemical nature of the residues in both active sites is globally unchanged, and this probably results in a similar binding of the phosphotriesters to *Sso*Pox active site (Fig. 2a). Both the PTEs and *Sso*Pox active sites are hydrophobic, around the binuclear center. The phosphotriester binding site organization is depicted in Fig. 2b. Small adjustments can be noted, such as the replacement of PTEs Trp131 and Phe132 with Tyr97 and Tyr99 in *Sso*Pox. Moreover, Tyr97 and Tyr99 are hydrogen bounded to each other via their side-chain oxygen atoms.

The chemical nature of the two metal cations of the active site was investigated using anomalous X-ray fluorescence (see Materials and Methods). For the *Sso*Pox crystals, the fluorescence spectrum analysis shows the presence of iron, cobalt, zinc, chloride and calcium ions (Fig. 3a). Chloride and calcium ions probably originate from the buffers used during the different steps from purification to crystallization, and no binding site has been detected for these ions by anomalous X-ray diffraction techniques. The three other metal cations have been described as part of the phosphotriesterase active site architecture.[9,10] This raises the question of the chemical nature of the metal cations that occupy the active site of *Sso*Pox. The problem was investigated using X-ray three-dimensional spectrometry (see Materials and Methods). Data were collected on a single *Sso*Pox crystal at two wavelengths: one higher and the other lower than the Co-K absorption edge (data not shown). Bijvoet difference Fourier maps (BDFM), calculated from data collected at 1.604 Å (lower than the Co-K edge), show two peaks on both α and β metals (Fig. 3a). This result totally excluded zinc because the wavelength used (1.604 Å) is above the Zn K edge (1.283 Å). At the wavelength above the Co-K edge (1.611 Å), the strong signal located on the α-metal disappeared (Fig. 3a), thus clearly identifying the β site as a cobalt ion. Concerning the α-site, the residual peak indicated the

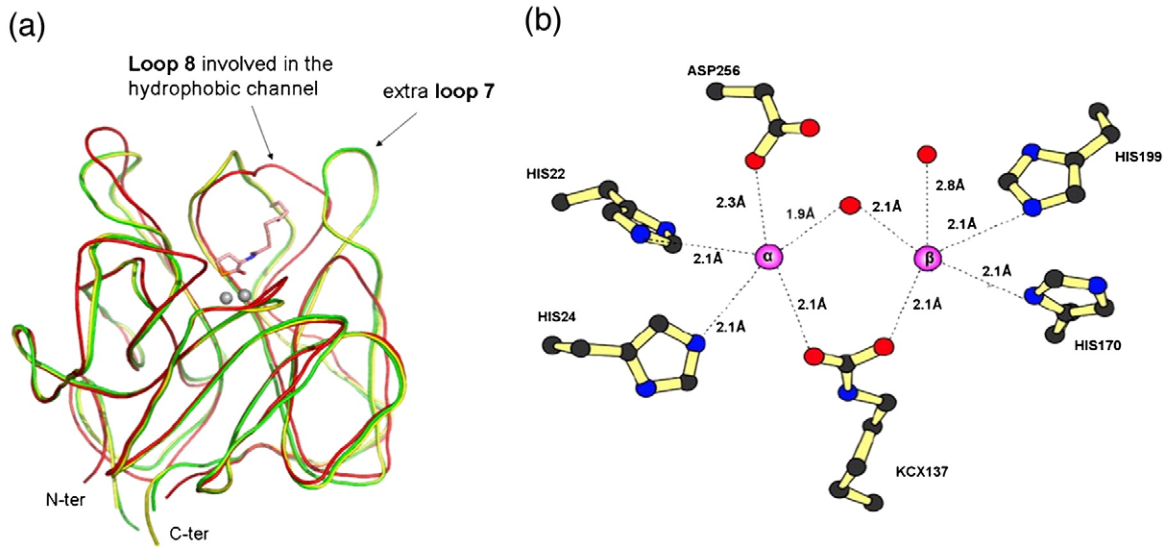

Fig. 1. *S. solfataricus* phosphotriesterase (PTE) structure. (a) Structural comparison of different known PTEs: hyperthermophilic *Sso*Pox in red, *P. diminuta* PTE in yellow and *A. radiobacter* PTE in green. The major structural differences, the absence of the 15 residue loop 7 in the *Sso*Pox structure, and loop 8 involved in the hydrophobic channel are shown by arrows. The C-terminal and N-terminal extremities of the backbones are indicated. The lactone mimic is shown by pink sticks, and the metals cations by grey balls. (b) A schematic view of the *Sso*Pox active site. Carbon, oxygen and nitrogen atoms are shown in black, red and blue, respectively. The purple balls indicate the metal cations labelled as α (iron) and β (cobalt). Distances are indicated in Å.

presence of only one other anomalous scatterer: an iron ion. This conclusion was confirmed by comparing the relative peak heights in the 1.604 Å wavelength BDFM. The α-site peak value (14σ) is about 85% of that of the β-site (16.5σ), a value very close to the anomalous scattering coefficient ratio of 87% between iron and cobalt at this wavelength†. The results show unambiguously that, using a purification protocol with Co^{2+}-containing buffers,[7] *Sso*Pox results in a protein with heterobinuclear centre constituted by an iron (α-site) and a cobalt cation (β-site), as was observed for *A. radiobacter* PTE.[12]

Description of the complexed structure

N-Decanoyl-L-homocysteine thiolactone (C10 HTL) is not a substrate for other members of the PLL family.[14] Here we confirm this observation for *Sso*Pox too and demonstrate that the thiolactone behaves as a competitive inhibitor towards *N*-octanoyl-L-homoserine lactone (C8 HSL), with a K_i at 25 °C of 432.7 (±53.2) μM against a K_M for C8 HSL of 174.4(±39.2) μM. The structure of *Sso*Pox in complex with this inhibitor was obtained at 2.05 Å resolution (Table 1). Although the *Sso*Pox fold is broadly similar to the other known PTEs, and the phosphotriester-binding site is comparable, the active site architecture is different. Indeed, loop 7 is shorter and loop 8 is longer (Fig. 1a). This creates a hydrophobic channel that elongates the phosphotriester substrate-binding site. This feature makes *Sso*Pox structurally different from the other mesophilic PTEs. Moreover, in the structure obtained with C10 HTL, this channel accommodates perfectly the added substrate analogue (Fig. 4). Despite the presence of Pro268, Pro272 and Pro276, the protruding loop 8 that constitutes this channel is probably more flexible than the rest of the structure, thus accommodating the substrate, as well as rigid enough for proper positioning. This consideration stems from the fact that the rmsd for Cα positions of residues in loop 8 between the free and in complex *Sso*Pox structure is 0.91 Å, revealing the entire loop to be involved in the substrate binding. More precisely, we defined two subsites: a large one that accommodates the substrate aliphatic chain, and a small one that positions the lactone ring. The aliphatic chain accommodates into the large subsite that forms the hydrophobic channel. Side chains of Phe229, Leu228, Leu226, Trp278, Ala266, Thr265, Ala275, Leu274 and side-chain carbon atoms of Lys271 make extensive van der Waals contacts with this substrate mimic. The thiolactone ring is positioned by polar and nonpolar interactions, just over the binuclear metal centre (Fig. 5).

The carbonyl oxygen of the ring interacts with the cobalt (β) cation (2.92 Å), with the hydroxyl group of Tyr97 (2.65 Å), and weakly with the Arg223 side chain (3.21 Å). The sulphur atom that mimics the oxygen of the lactone ring is bound to the iron (α) ion (3.23 Å). Side chains of Arg223, Leu72, Val27, Ile261 and Trp263 position the rest of the ring. The indole ring of Trp263 is just above the substrate ring, in the van der Waals interaction, and a large movement of this residue occurs while the substrate is bound. The carbonyl oxygen of the substrate peptide linkage contacts the Cys258 side chain (3.89 Å). In addition, the putative catalytic bridging water is not equidi-

† http://skuld.bmsc.washington.edu/scatter/

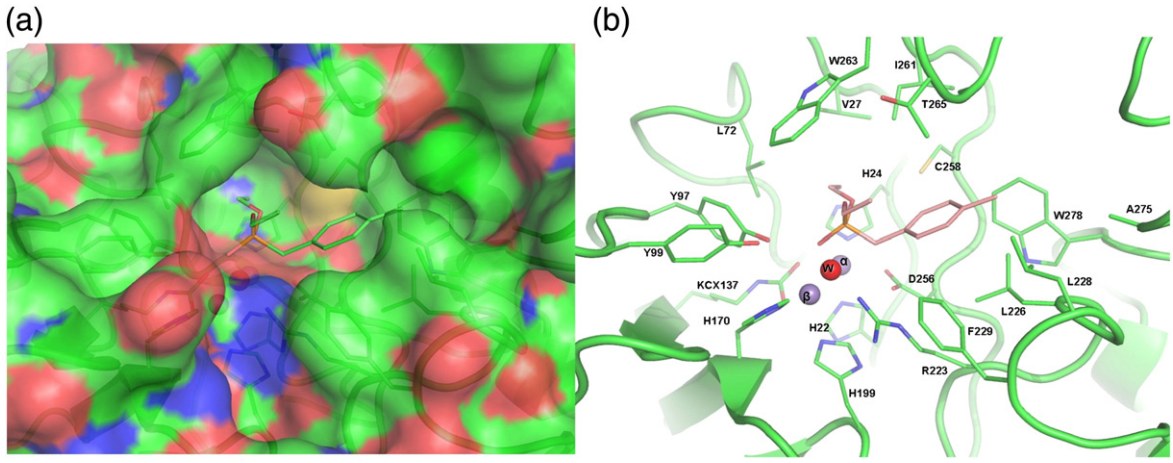

Fig. 2. Docking of a phosphotriester mimic in the active site of *Sso*Pox. (a) The phosphotriester mimic (shown by green sticks) and the molecular surface of the structure of *Sso*Pox are indicated. (b) The phosphotriester mimic and the residues in contact with it are shown by pink and green sticks, respectively.

stant from both metal cations (Fig. 5), but closer to the iron cation (α) (2.06 Å and 2.61 Å to α and β, respectively). Its position appears to be optimized for a nucleophilic attack on the carbonyl carbon of the lactone ring. Indeed, this bridging water molecule is close to the sp2 carbon (2.40 Å) and almost perpendicular to its plane.

Further investigation shows an impressive structural similarity between the $(\beta/\alpha)_8$ folded *Sso*Pox and *B. thuringiensis* AHL lactonase (AiiA) active sites (Fig. 6). This lactonase belongs to the metallo-β-lactamases superfamily,[18] possesses the conserved motif HXHXDH, and shares the characteristic fold of this family: αβ / βα. The structural comparison of *Sso*Pox with AiiA allowed us to identify a key residue that serves to position the lactone ring above the binuclear center: Tyr97 and Tyr194 in *Sso*Pox and in AiiA, respectively. In addition, other key elements for the catalytic reaction, namely, metal cations and the putative catalytic water molecule, as well as the aspartic acid that positions the water molecule, are extremely similar in both *Sso*Pox and AiiA. However, *Sso*Pox and AiiA do not share a significant sequence identity, possess different folds and no common metal cation-binding motifs (see Discussion). These two proteins are good examples of convergent evolution.

Mutagenesis approach

We used mutagenesis to analyze further the role of putative key residues in the *Sso*Pox active site. Arg223 in the structure of *Sso*Pox corresponds to the *P. diminuta* PTE His254, a residue potentially involved in a proton transfer according to the PTE mechanism suggested previously.[13] The PTE from *A. radiobacter* possesses an Arg at this position (Arg254) and this residue was shown to interact with the substrates.[12] In the case of *Sso*Pox, kinetic studies detected a large decrease in the paraoxonase and lactonase catalytic activity of the mutant R223H, probably resulting in the loss of an interaction with the substrates (Table 2). The residue Tyr97, involved in the complex with the lactone mimic, was also mutated. For the Y97W mutant, we observed a threefold increase in both activities without any effect on K_M (Table 2).

Discussion

Catalytic mechanisms for the hyperthermophilic *Sso*Pox

Phosphotriesterase activity

A phosphotriesterase mechanism was proposed by Aubert *et al.*[13] In particular, the authors suggested the existence of a proton transfer in *P. diminuta* PTE. In brief, Asp301 is thought to deprotonate the pentacoordinated intermediate and the proton is subsequently shuttled away from the active site with the assistance of His254 and Asp233. This proton pathway mechanism has been ruled out by QM/MM simulations,[19] and previously published mutagenesis studies performed on *P. diminuta* PTE revealed that mutations H254G/R showed no drastic effect on catalysis.[20–22] In addition, His254 is not conserved within the PTE family and is replaced by an arginine in the very active mesophilic PTE from *A. radiobacter*.[21] The *Sso*Pox structure is compatible with these observations: *Sso*Pox also possesses an arginine (Arg223) in place of this histidine, and the recovery of the side chain involved in the hypothetical proton transfer pathway with the R223H mutant does not increase *Sso*Pox phosphotriesterase activity. The *Sso*Pox structure and its docking with a phosphotriester mimic allow us to propose a mechanism (Fig. 7a) compatible with that recently proposed by Wong and co-workers.[19]

*Sso*Pox possesses a heterobinuclear iron / cobalt centre. According to our models, this binuclear centre is utilized to activate the catalytic water molecule to a hydroxide ion, as for the mesophilic PTEs [23] and *Sso*Pox lactonase (see below). When the substrate is in

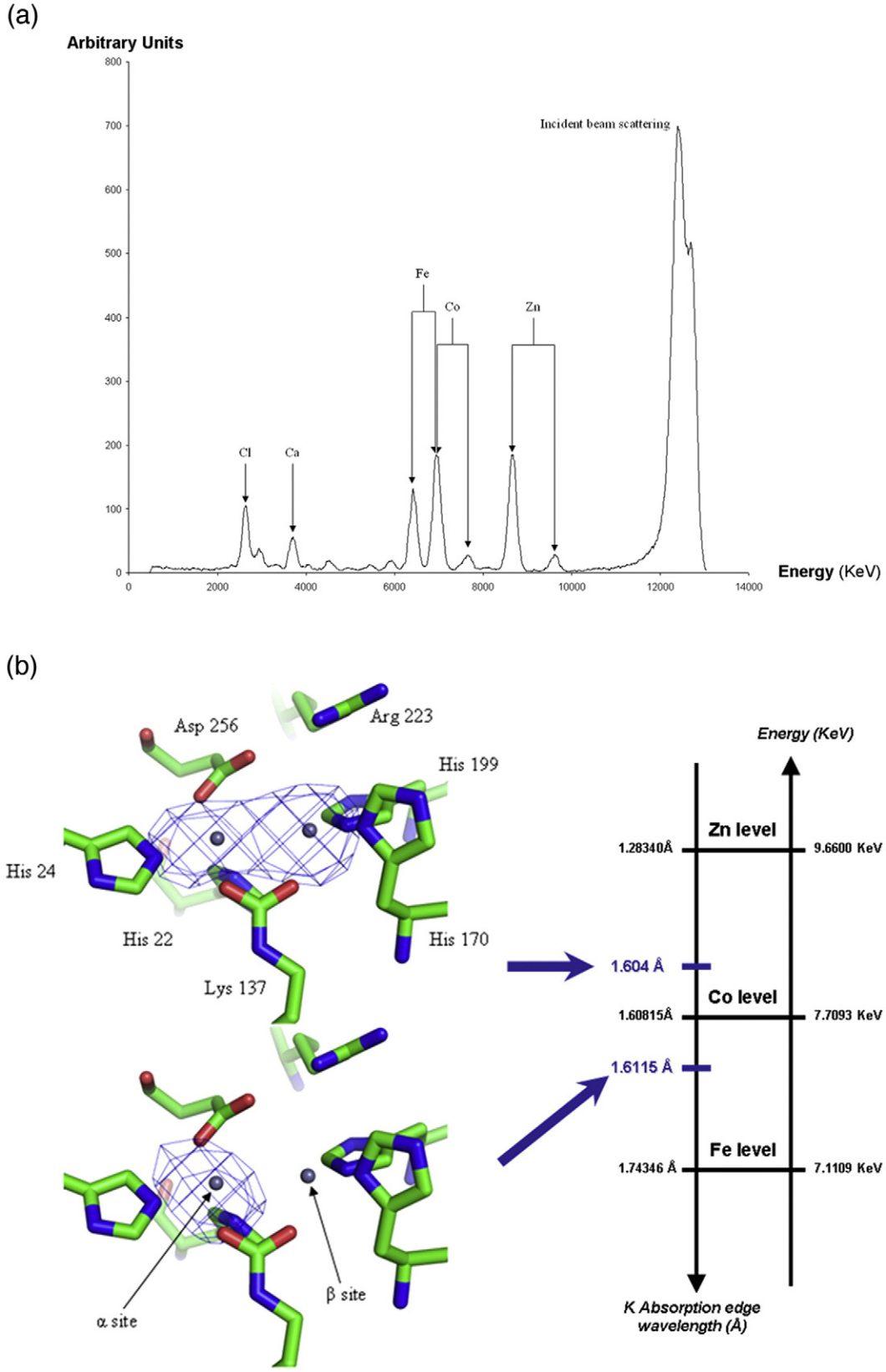

Fig. 3. Anomalous scattering discriminates between metals in the *Sso*Pox active site. (a) X-ray fluorescence spectrum measured on a single *Sso*Pox crystal at beamline FIP-BM30A of ESRF. This spectrum shows the presence of many ions: iron, cobalt, zinc, calcium and chloride. Doubled arrows for iron, cobalt and zinc indicate characteristic absorption Kα and Kβ edges. Simple arrows indicate calcium and chloride on the spectrum. (b) Final model and Bijvoet difference Fourier maps contoured at 3σ; on the left is the map corresponding to data collected at 1.604 Å and on the right the map corresponding to data collected at 1.6115 Å. The maps were calculated using the full resolution range. This clearly demonstrates that the α site is occupied by an iron cation and the β site by a cobalt cation.

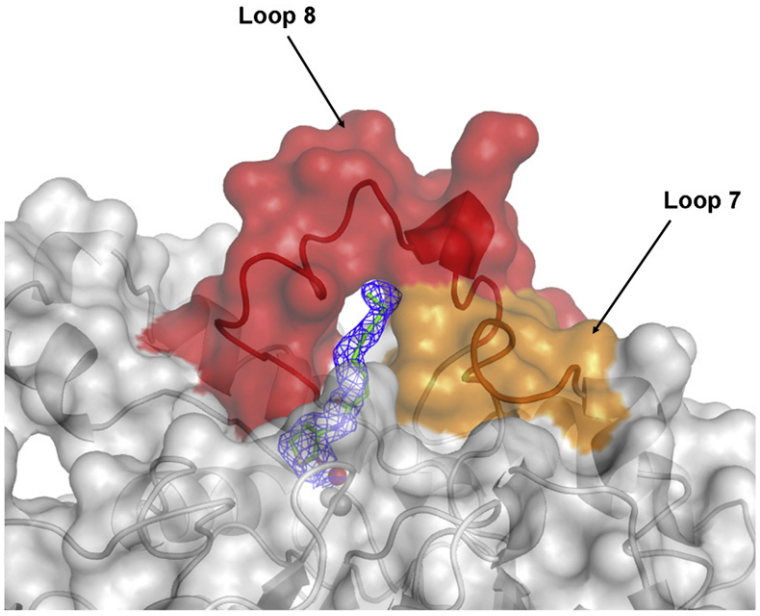

Fig. 4. Active site topology. The active site cavity: loop 8 is highlighted in red and loop 7 in orange. The lactone mimic is highlighted by green sticks; the metals cations are shown by grey balls, and the putative catalytic water molecule by red ball. The electronic density map $F_o - F_c$ in blue was calculated omitting the substrate mimic and contoured at 3σ. Arrows indicate the active site loops.

complex with the binuclear centre, the hydroxide ion attacks the electrophilic phosphorus centre via the S_N2 mechanism, forming a pentacoordinated transition state that bridges the two metals. The binuclear centre, especially the cobalt cation (β), compensates for the developing negative charge on the phosphoryl oxygen. The electron pair of the phosphoryl oxygen folds back to the phosphorus-oxygen bond, thus allowing the leaving group to be released. The bridging phosphorus moiety is expelled from the active site and replaced by a water molecule from the solvent bulk, thus regenerating the enzyme.

Lactonase activity

Taking into account the binding of the substrate analogue C10 HTL to *Sso*Pox, considering its behaviour as a competitive inhibitor towards the quorum-sensing substrate C8 HSL, and keeping in mind the refined phosphotriesterase mechanism proposed above (Fig. 7a), we also now propose a lactonase mechanism (Fig. 7b).

The hydrophobic channel accommodates the acyl chain of the substrate, whereas the lactone ring is positioned above the binuclear centre. The thiolactone ring sulphur and the carbonyl oxygen of the substrate mimic interact with the iron (α) and the cobalt cation (β), respectively. This results in an enhanced polarization of the carbonyl bond, making it more susceptible to a nucleophilic attack, in a way similar to that described for phosphorus-oxygen polarization in phosphotriester hydrolysis. The carbonyl oxygen accepts the Tyr97 hydroxyl hydrogen. This Tyr residue appears to be involved in the adjustment of the lactone ring. Interestingly, in lactone hydrolase, which belongs to the metallo-β-lacta-

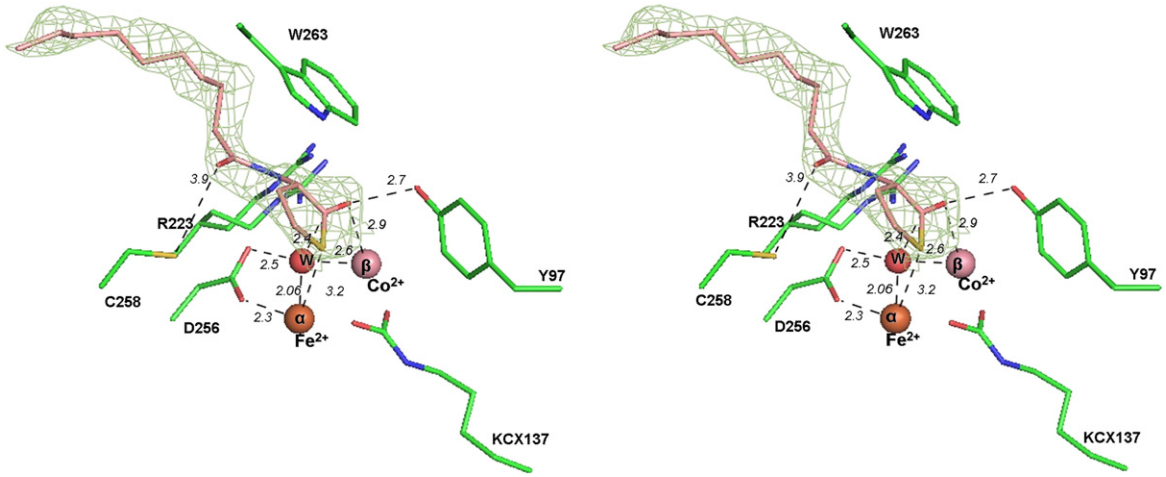

Fig. 5. *Sso*Pox in complex with the lactone mimic. Close and stereo view into the binding of the thiolactone ring. The protein side chains are shown by green sticks. The different electronic density map calculated by omitting the lactone mimic is shown in the green grid and contoured at 3 σ. R223 is shown as two equally likely conformations. The lactone mimic is shown by pink sticks. The putative catalytic water molecule, the iron ion (α) and the cobalt (β) ion are shown by red, orange and purple spheres respectively. Distances are indicated in Å.

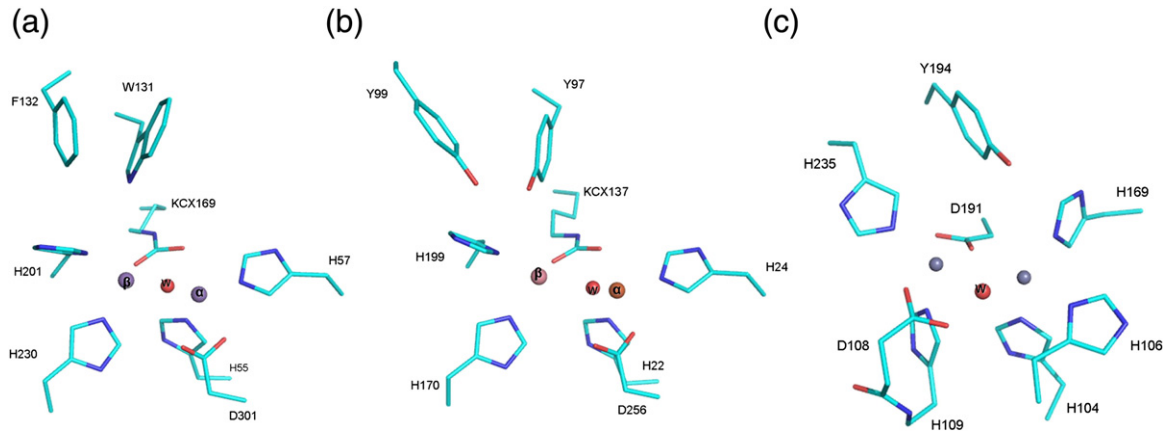

Fig. 6. Active site comparison. (a) Active site view of the *Pseudomonas diminuta* PTE (PDB ID 1DPM). (b) Active site view of *Sso*Pox. (c) Active site view of the *Bacillus thuringiensis* AHL lactonase (PDB ID 2A7M). Amino acids are shown by sticks, zinc cations by grey balls, the cobalt cation by a purple ball, the iron cation by an orange ball, and the putative catalytic water molecule by red balls.

mases superfamily,[18] Tyr194 has a similar role in positioning the substrate (Fig. 5), and is conserved in this lactonase family. In *Sso*Pox, the bridging hydroxide ion interacts strongly with the iron cation (α) and with Asp256, and is positioned ideally for a nucleophilic attack on the carbonyl carbon, as this molecule is almost perpendicular to the carbonyl plane. Furthermore, this water is no longer equidistant from both metals as observed in the free structure, but is closer to the iron cation (α). This strong interaction makes very good sense from a physiological perspective: the pK_a of Fe^{2+}-H_2O is significantly lower than that of Zn^{2+}-H_2O and Co^{2+}-H_2O (6.7 *versus* 9.0 and 8.9, respectively), making it the most efficient Lewis acid in the physiological pH range,[12] and allowing it to activate efficiently this water molecule. Because of this nucleophilic attack on the substrate carbonyl atom, a negatively charged transition state is formed, primarily stabilized by interactions with the cobalt cation (β) and the Tyr97 hydroxyl. In contrast to the phosphotriester hydrolysis, this transition state does not adopt a pentacoordinate geometry, but rather a tetrahedral geometry. Then, the electron pair of the carbonyl oxygen folds back on the carbonyl carbon, thus breaking the carbon–oxygen bond of the lactone ring. The hydrolysis product is released and the enzyme is thus regenerated. This mechanism resembles that recently proposed for quorum-quenching lactonase (AiiB) from *Agrobacterium tumefaciens*.[24] In this case too, the bridging hydroxide has been proposed to be the nucleophile. We have proposed basically the same mechanism for the phospotriesterase activity (Fig. 6a). However, the precise phosphotriesterase mechanism is still under debate as a recent article has proposed a different scheme for the nucleophilic attack.[25]

The structure of the complex does not reveal clearly a residue potentially capable of protonating the leaving alcohol anion, even though Cys258 may potentially fulfil this role (see Results).

Relationship between both mechanisms

The catalytic properties of *Sso*Pox,[14] and our results confirm that the phosphotriesterase activity could be extremely high, even without compromising the lactonase activity, and probably *vice versa*. Considering the two mechanisms proposed, the hydrolysis of these

Table 2. Kinetic parameters of *Sso*Pox wild type and mutants with paraoxon or 5-thiobutyl-γ-butyrolactone

	P. diminuta PTE (Zn/Zn)	*S. solfataricus* *Sso*Pox						*B. thuringiensis* AiiA
	Phosphotriesterase	Phosphotriesterase			Lactonase			Lactonase
	Paraoxon	Paraoxon			5-Thiobutyl-γ-butyrolactone			3-Oxo-C8-HSL
	Wild type[a]	Wild type[b]	R223H	Y97W	Wild type[c]	R223H	Y97W	Wild type[d]
k_{cat} (s^{-1})	2300±150	0.24±0.01	n.d.	0.68±0.04	29.0±7.0	0.420±0.004	75.7±8.0	22.17
K_M (mM)	0.078±0.008	0.060±0.009	n.d.	0.075±0.007	0.080±0.003	0.273±0.059	0.079±0.015	2.28
k_{cat}/K_M (s^{-1} mM^{-1})	30000±2000	4.00±0.75	0.0037±0.18[e]	9.0±0.3	360.0±90.0	1.54±0.31	958.2±172.4	9.72

[a] Data were taken from Ref. 11.
[b] Data for wild type were taken from Ref. 7.
[c] Data for wild type were taken from Ref. 14.
[d] Data for wild type were taken from Ref. 34.
[e] Deduced from subsaturating conditions. For paraxonase activity, as paraoxon was not saturating up to 5 mM we could only estimate the catalytic efficiency ($s = k_{cat}/K_M$) under pseudo first-order conditions (e.g. $[S] << K_M$) and compare data with wild type values.

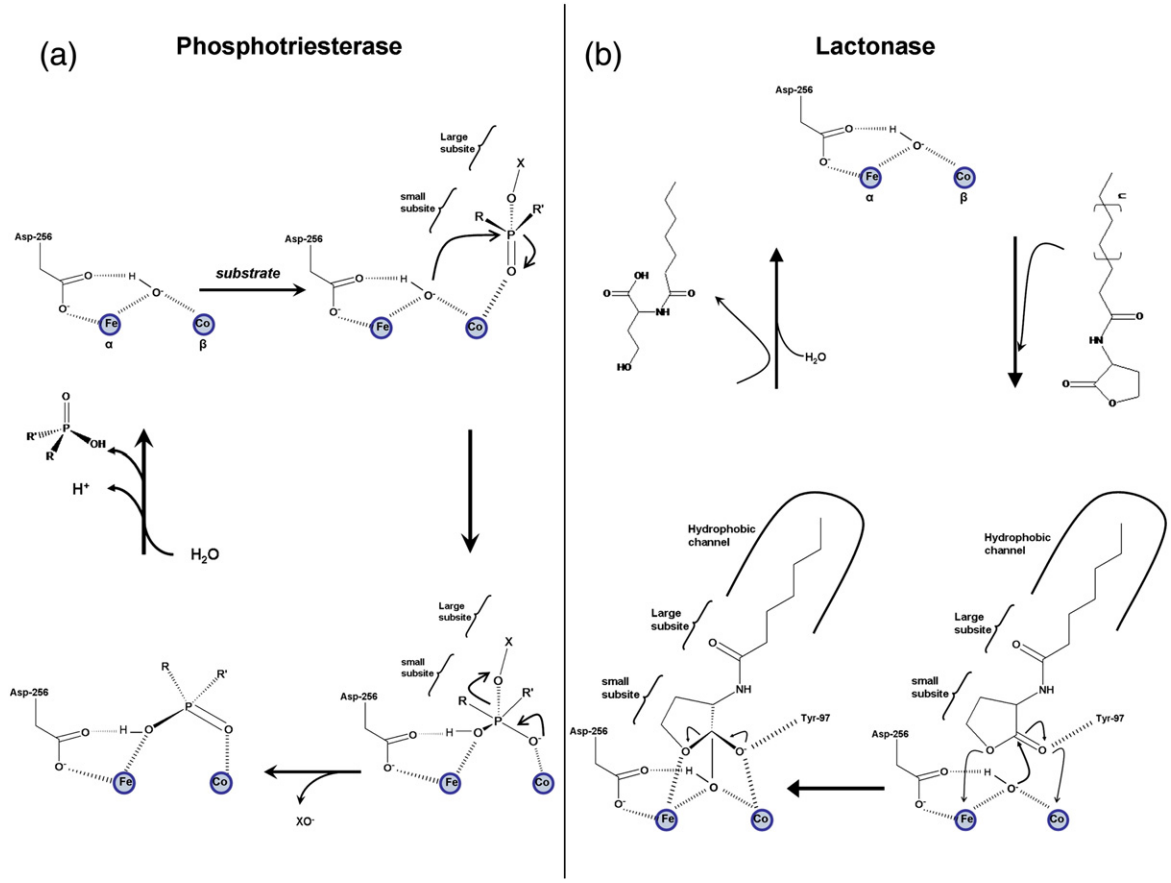

Fig. 7. Proposed catalytic mechanism. (a) A model for the chemical reaction mechanism of phosphotriesterases. (b) Model for the chemical reaction mechanism of *Sso*Pox lactonase activity. Small and large sites are indicated in accordance with the PTE nomenclature.[17]

two substrates requires common primary features: the binuclear centre and the bridging catalytic hydroxide ion. Regarding chemistry, the hydrolysis of the lactones implies an sp3 transition state, whereas the hydrolysis of a phosphotriester proceeds *via* the formation of a pentacoordinated transition state. The fact that *Sso*Pox is capable of accommodating both intermediate species is an interesting feature, as enzymes are generally said to stabilize transition states specifically.[26]

Several lactonases with scaffolds completely different from that of *Sso*Pox, are already known, and all exhibit, albeit with lower efficiency, promiscuous phosphotriesterase activity (AHL lactonase from *B. thuringiensis* [14] and the mammalian PONs [27]). On the phosphotriesterase side, bacterial PTEs exhibit promiscuous lactonase activity.[22] As these enzymes exhibit both lactonase and phosphotriesterase activities, this suggests that the promiscuous phosphotriesterase activity could stem from a certain overlap between the transition states of lactone and phosphotriester hydrolysis. Furthermore, other hydrolases that proceed *via* sp3 transition states, such as esterase (carboxylesterase [28]) and prolidase,[29] also possess promiscuous phosphotriesterase activity. From these observations, it seems that if an enzyme is capable of producing an adequate nucleophilic attack and is apt to stabilize an sp3 transition state, it would also be capable of accommodating a pentacoordinated transition state, albeit with lower efficiency. Then, optimization in a reaction for a specific substrate is achieved by chemical environmental adaptation for the proper binding and positioning of the substrate, and stabilization of the transition state. This promiscuity in chemistry is probably an important reservoir in enzymatic activity creation.

Structural adaptation between lactonases and phosphotriesterases

Lactonases with promiscuous phosphotriesterase activity such as PPLs are thus a tangible link to mesophilic PTEs.[14] The structural comparison between bacterial PTEs and *Sso*Pox reveals adjustments in the small sub-site, like the replacement of Tyr97 and 99 in *Sso*Pox by Trp131 and Phe132 in PTEs respectively. The role of Tyr97 seems to be in the positioning of the substrate lactone ring. Accordingly, mutation Y97W, which was made to mimic the mesophilic PTE structures, results in a threefold increase in paraoxonase and lactonase activity and specificity. For the large sub-site, the extra loop 7 of the PTEs, which forms a short α-helix, completely blocks the channel that is created by loop 8 in *Sso*Pox, and narrows the binding site. The smaller cavity that is created adjusts well to the hydrophobic leaving groups of phosphotriesters.

This structural work suggests loop grafting is required to diverge from a lactonase to an optimized phosphotriesterase activity. On the lactonase side, the *Sso*Pox structure shows a long hydrophobic channel able to accommodate the acyl chains of the lactones. This particular binding site and the key tyrosine residue that positions the substrate seem to be important for the hydrolysis of the aliphatic lactones and maybe for the substrate specificity. Indeed, the AiiA from *B. thuringiensis* does possess a hydrophobic channel and a tyrosine residue (Tyr194, see Fig. 6), which is conserved among this lactonase family and with the same function, providing a good illustration of convergent evolution. To conclude, *Sso*Pox possesses an optimized binding site for aliphatic lactones, and the central part of this cavity is sterically and chemically close to the binding site of the optimized phosphotriesterase, allowing *Sso*Pox to carry out both activities.

Materials and Methods

Crystallization

The cloning, expression, and purification of the recombinant *Sso*Pox in *Escherichia coli* have been described.[7] The enzyme was concentrated to 5.8 mg.mL^{-1}. Crystallization was performed using the hanging-drop, vapour-diffusion method.[30] Equal volumes (0.5–1 μL) of protein and reservoir solutions were mixed, and the resulting drops were equilibrated against a 800 μL reservoir solution containing 15–18% (w/v) PEG 8000 and 50 mM Tris–HCl buffer (pH 8). Thin crystals appeared after one week at 277 K. Co-crystallization assays with C10 HTL were performed using the same protocol and by adding 1μL of the 50 mM thiolactone solution (ethyl acetate:DMSO; 1:1) to 30μL of the protein solution. *Sso*Pox crystals appeared instantaneously after mixing the protein and reservoir solutions.

Data collection

The crystals were first transferred to a cryoprotectant solution composed of the reservoir solution and 25% (v/v) glycerol. For the co-crystallized crystals, 1 μL of the thiolactone solution was added to the cryoprotectant solution. Each crystal was then flash-cooled in liquid nitrogen. For the native structure, X-ray diffraction data were collected at 100 K using synchrotron radiation at the FIP BM30A beam line (ESRF, Grenoble, France) using a MarCCD (165 mm) detector. A data set was recorded at 2.6 Å resolution (Table 1). For co-crystallized crystals, X-ray diffraction data were collected at 100 K using synchrotron radiation at the ID14-1 beam line (ESRF, Grenoble, France) using a ADSC Q210 CCD detector. A data set was recorded at 2.05 Å resolution (Table 1).

Structure determination

X-ray diffraction data were integrated, scaled and merged with the XDS program [31] and the CCP4 program suite.[32] Initial molecular replacement was performed with Phaser,[33] using a polyalanine model deduced from the structure of the *P. diminuta* PTE from 1DPM [14] as described.[30] Two protein molecules were found in the asymmetric unit (translation-function *Z* scores of 7.22 and 6.72). Given the molecular mass of *Sso*Pox (35.5 kDa), this corresponds to a high Matthews coefficient (V_M) of 5.0 Å^3 Da^{-1} and a high solvent content of approximately 75.2% (v/v). The electron-density map calculated with model phases obtained from molecular replacement was of poor quality. Very few of the side chains were visible in the maps. Nevertheless, the active site, composed of two metal cations, was already clearly visible. The electron-density map was improved with DM,[33] using solvent flattening and noncrystallographic symmetry averaged between the two molecules. Manual model improvement was performed using Coot.[32] Using the improved model and fixing the two initial solutions, molecular replacement was performed using MOLREP,[32] producing two extra solutions, giving a total of four protein molecules in the asymmetric unit (R_{cryst} = 0.47, correlation coefficient = 0.325). This corresponds to a V_M of 2.5 Å^3 Da^{-1}, which is a more typical value. Finally, the new electron-density maps were of sufficient quality for model building.

X-ray fluorescence

An X-ray fluorescence spectrum was acquired with a solid-state Röntec XFlash detector operating at the beam line FIP-BM30A (ESRF, Grenoble, France). The fluorescence detector for analysis of the absorption-edge structure was placed 90° from the incident X-ray beam to minimize scattering. This technique allows us to identify all the atoms with an absorption edge lower than the incident X-ray beam energy. All scatterers will fluoresce with a characteristic energy, depending on the nature of the atom. This reveals the presence of any anomalous scatterers present in the whole sample, i.e protein and solvent.

Three-dimensional spectrometry

In order to locate only ordered scatterers, diffraction data were collected and BDFM maps were calculated. To identify the chemical nature of the scatterers, two data collections were processed at a higher and lower energy level than the absorption edge characteristic of one atom. If the signal disappears, this characterizes unambiguously the atom nature. Finally, this technique has the power to identify unambiguously the chemical nature of ordered atoms and allows their location spatially in the protein structure.

For the *Sso*Pox crystals, two complete anomalous datasets, consisting of 360×1° oscillations, were collected at 2.9 Å resolution at the BM14 beam line (ESRF, Grenoble, France), at wavelengths lower (1.604 Å) and higher (1.611 Å) than the Co-K absorption edge (1.608 Å).

Docking

A phosphotriester mimic (diethyl-4-methylbenzylphosphonate) was manually docked to the *Sso*Pox structure based on the structure of *P. diminuta* (PDB CODE 1DPM).

Figures. The stereo and ribbon representations of the *Sso*Pox structure shown in the Figs. were made using PyMOL‡.

Site-directed mutagenesis

Mutant derivatives of the *ssopox* gene were prepared by PCR mutagenesis. Plasmid pT7-7 (a derivative of pBR322; Stratagene) carrying wild-type *ssopox* was used as a template for amplification reactions carried out with a high-

‡ http://www.pymol.org

fidelity *Pfu*-turbo DNA polymerase (Stratagene), using complementary pairs of mutagenic oligonucleotides. The oligonucleotides used were:

R223Hfor, 5′-ATTGGATTAGATCATTATGGTTTAG-3′
R223Hrev, 5′-CTAAACCATAATGATCTAATCCAAT-3′

PCR reactions were performed as follows: first round 94 °C/4 min, followed by 30 cycles of 92 °C for 1 min, 54 °C for 1 min, 72 °C for 5 min and a final elongation step of 72 °C for 10 min. An aliquot of the amplified DNA products was digested with *Dpn*I (37 °C for 60 min) to degrade the template (methylated DNA). *E. coli* strain TOP10 was transformed with the newly synthesized linear plasmid, and the plasmid was purified from one of the resulting colonies. Sequencing was performed to exclude any unwanted mutation. Preparation of the Y97W mutant and its characterization will be reported in detail elsewhere.

Protein expression, purification and characterization

The mutant R223H was expressed in *E. coli*, purified and characterized essentially as described.[7] The kinetic parameters for R223H and Y97W were measured as described [7,14] for paraoxonase and lactonase activity, respectively.

Inhibition study on *N*-decanoyl L-homocysteine thiolactone

The Michaelis–Menten constant for the C8 HSL substrate was evaluated over the range 0.04–0.6 mM. The hydrolysis of the substrate was evaluated by pH-sensitive colorimetric assay,[35] monitoring the decrease of the pH indicator absorbance. The reactions were performed in 1 mM tricine buffer (pH 8.05) at 25 °C, 1.5% (v/v) DMSO, using 0.2 mM purple cresol as the indicator. The decrease in absorbance at 572 nm was measured in a microtiter plate reader (VICTOR™3; PerkinElmer). The initial velocity substrate concentration data were fit to the Lineaweaver–Burk transformation of the Michaelis–Menten equation by weighted linear least-squares analysis with a personal computer and the GRAFIT program (version 3.0. Erithacus SoftwareLtd, Staines, UK).

The study of the *N*-decanoyl-L-homocysteine thiolactone inhibitory effect (K_i) was performed by evaluation of the effects of 90 μM, 180 μM and 360 μM inhibitor on the Michaelis-Menten C8HSL curves (as described above). The data were used to create Lineweaver–Burk plots and the slopes of the three lines were re-plotted against the concentration of inhibitor to calculate K_i.

Protein Data Bank accession codes

The atomic coordinates and structural factors of the free *Sso*Pox and its complex with the *N*-decanoyl-L-homocysteine thiolactone have been deposited with the Protein Data Bank with accession codes 2VC5 and 2VC7, respectively.

Acknowledgements

We are very grateful to Drs Dan S. Tawfik and Olga Khersonsky for providing the substrate TBBL and C10 HTL inhibitor. This research was supported by grants to P.M. and E.C. by the Délégation Générale pour l'Armement (CO n°010807/03-10) and by the C.N.R.S. We thank the MIUR project Piano Nazionale Ricerca per le Biotecnologie Avanzate II –Biocatalisi and the DNA Sequencing Core of TIGEM-IGB for sequencing mutants.

References

1. Raushel, F. M. (2002). Bacterial detoxification of organophosphate nerve agents. *Curr. Opin. Microbiol.* **5**, 288–295.
2. LeJeune, K. E., Wild, J. R. & Russell, A. J. (1998). Nerve agents degraded by enzymatic foams. *Nature*, **395**, 27–28.
3. Seibert, C. M. & Raushel, F. M. (2005). Structural and catalytic diversity within the amidohydrolase superfamily. *Biochemistry*, **44**, 6383–6391.
4. Munnecke, D. M. (1976). Enzymatic hydrolysis of organophosphate insecticides, a possible pesticide disposal method. *Appl. Environ. Microbiol.* **32**, 7–13.
5. Sethunathan, N. & Yoshida, T. A. (1973). Flavobacterium sp. that degrades diazinon and parathion. *Can. J. Microbiol.* **1-9**, 873–875.
6. Horne, I., Qiu, X., Russell, R. J. & Oakeshott, J. G. (2003). The phosphotriesterase gene opdA in Agrobacterium radiobacter P230 is transposable. *FEMS Microbiol. Lett.* **222**, 1–8.
7. Merone, L., Mandrich, L., Rossi, M. & Manco, G. A. (2005). Thermostable phosphotriesterase from the archaeon Sulfolobus solfataricus: cloning, overexpression and properties. *Extremophiles*, **9**, 297–305.
8. Ghanem, E. & Raushel, F. M. (2005). Detoxification of organophosphate nerve agents by bacterial phosphotriesterase. *Toxicol. Appl. Pharmacol.* **207**, 459–470.
9. Benning, M. M., Shim, H., Raushel, F. M. & Holden, H. M. (2001). High resolution X-ray structures of different metal-substituted forms of phosphotriesterase from Pseudomonas diminuta. *Biochemistry*, **40**, 2712–2722.
10. Jackson, C., Kim, H. K., Carr, P. D., Liu, J. W. & Ollis, D. L. (2005). The structure of an enzyme-product complex reveals the critical role of a terminal hydroxide nucleophile in the bacterial phosphotriesterase mechanism. *Biochim. Biophys. Acta*, **1752**, 56–64.
11. Omburo, G. A., Kuo, J. M., Mullins, L. S. & Raushel, F. M. (1992). Characterization of the zinc binding site of bacterial phosphotriesterase. *J. Biol. Chem.* **267**, 13278–13283.
12. Jackson, C. J., Carr, P. D., Kim, H. K., Liu, J. W., Herrald, P., Mitić, N. *et al.* (2006). Anomalous scattering analysis of Agrobacterium radiobacter phosphotriesterase: the prominent role of iron in the heterobinuclear active site. *Biochem. J.* **397**, 501–508.
13. Aubert, S. D., Li, Y. & Raushel, F. M. (2004). Mechanism for the hydrolysis of organophosphates by the bacterial phosphotriesterase. *Biochemistry*, **43**, 5707–5715.
14. Afriat, L., Roodveldt, C., Manco, G. & Tawfik, D. S. (2006). The latent promiscuity of newly identified microbial lactonases is linked to a recently diverged phosphotriesterase. *Biochemistry*, **45**, 13677–13686.
15. Parsek, M. R. & Greenberg, E. P. (2005). Sociomicrobiology: the connections between quorum sensing and biofilms. *Trends Microbiol.* **13**, 27–33.
16. Vanhooke, J. L., Benning, M. M., Raushel, F. M. & Holden, H. M. (1996). Three-dimensional structure of the zinc-containing phosphotriesterase with the bound substrate analog diethyl 4-methylbenzylphosphonate. *Biochemistry*, **35**, 6020–6025.

17. Chen-Goodspeed, M., Sogorb, M. A., Wu, F., Hong, S. B. & Raushel, F. M. (2001). Structural determinants of the substrate and stereochemical specificity of phosphotriesterase. *Biochemistry*, **40**, 1325–1331.
18. Liu, D., Lepore, B. W., Petsko, G. A., Thomas, P. W., Stone, E. M., Fast, W. & Ringe, D. (2005). Three-dimensional structure of the quorum-quenching N-acyl homoserine lactone hydrolase from Bacillus thuringiensis. *Proc. Natl Acad. Sci. USA*, **102**, 11882–11887.
19. Wong, K. Y. & Gao, J. (2007). The reaction mechanism of paraoxon hydrolysis by phosphotriesterase from combined QM/MM simulations. *Biochemistry*, **46**, 13352–13369.
20. Hill, C. M., Li, W. S., Thoden, J. B., Holden, H. M. & Raushel, F. M. (2003). Enhanced degradation of chemical warfare agents through molecular engineering of the phosphotriesterase active site. *J. Am. Chem. Soc.* **125**, 8990–8991.
21. Yang, H., Carr, P. D., McLoughlin, S. Y., Liu, J. W., Horne, I., Qiu, X. *et al.* (2003). Evolution of an organophosphate-degrading enzyme: a comparison of natural and directed evolution. *Protein Eng.* **16**, 135–145.
22. Roodveldt, C. & Tawfik, D. S. (2005). Shared promiscuous activities and evolutionary features in various members of the amidohydrolase superfamily. *Biochemistry*, **44**, 12728–12736.
23. Samples, C. R., Howard, T., Raushel, F. M. & DeRose, V. J. (2005). Protonation of the binuclear metal center within the active site of phosphotriesterase. *Biochemistry*, **44**, 11005–11013.
24. Liu, D., Thomas, P. W., Momb, J., Hoang, Q. Q., Petsko, G. A., Ringe, D. & Fast, W. (2007). Structure and specificity of a quorum-quenching lactonase (AiiB) from Agrobacterium tumefaciens. *Biochemistry*, **46**, 11789–11799.
25. Jackson, C. J., Foo, J. L., Kim, H. K., Carr, P. D., Liu, J. W., Salem, G. & Ollis, D. L. (2008). In crystallo capture of a Michaelis complex and product-binding modes of a bacterial phosphotriesterase. *J. Mol. Biol.* **375**, 1189–1196.
26. Schramm, V. L. (1998). Enzymatic transition states and transition state analog design. *Annu. Rev. Biochem.* **67**, 693–720.
27. Draganov, D. I., Teiber, J. F., Speelman, A., Osawa, Y., Sunahara, R. & La Du, B. N. (2005). Human paraoxonases (PON1, PON2, and PON3) are lactonases with overlapping and distinct substrate specificities. *J. Lipid Res.* **46**, 1239–1247.
28. Maxwell, D. M. & Brecht, K. M. (2001). Carboxylesterase: specificity and spontaneous reactivation of an endogenous scavenger for organophosphorus compounds. *J. Appl. Toxicol.* **21**(Suppl. 1), S103–S107.
29. Cheng, T. C., Harvey, S. P. & Stroup, A. N. (1993). Purification and properties of a highly active organophosphorus acid anhydrolase from Alteromonas undina. *Appl. Environ. Microbiol.* **59**, 3138–3140.
30. Elias, M., Dupuy, J., Merone, L., Lecomte, C., Rossi, M., Masson, P. *et al.* (2007). Crystallization and preliminary X-ray diffraction analysis of the hyperthermophilic Sulfolobus solfataricus phosphotriesterase. *Acta Crystallogr.* **63**, 553–555.
31. Kabsch, W. (1993). Automatic processing of rotation diffraction data from crystals of initially unknown symmetry land cell constants. *J. Appl. Crystallogr.* **26**, 795–800.
32. Collaborative Computational Project Number 4. (1994). The CCP4 suite: programs for protein crystallography. *Acta Crystallogr. D*, **50**, 760–763.
33. Cowtan, K. D. & Zhang, K. Y. (1999). Density modification for macromolecular phase improvement. *Prog. Biophs. Mol. Biol.* **72**, 245–270.
34. Wang, L. H., Weng, L. X., Dong, Y. H. & Zhang, L. H. (2004). Specificity and enzyme kinetics of the quorum-quenching N-Acyl homoserine lactone lactonase (AHL-lactonase). *J. Biol. Chem.* **279**, 13645–13651.
35. Chapman, E. & Wong, C. H. (2002). A pH sensitive colorimetric assay for the high-throughput screening of enzyme inhibitors and substrates: a case study using kinases. *Bioorg. Med. Chem.* **10**, 551–555.